

Radioimmunotherapy of Metastatic Melanoma

Introduction

Radioimmunotherapy is the process of binding an antibody to a tumor-associated antigen to deliver a lethal dose of radiation to tumor cells. The efficacy of RIT as a skin cancer treatment is dependent on the tumor depth that the radiolabeled antibody can penetrate and thus bind to melanin binding sites to emit cytotoxic doses of radiation that kill melanoma cells. This study developed three-dimension (3D) and 1-dimensional (1D) models of the radiolabeled antibody's interaction with tumor melanin to gain insight into the pharmacokinetics of RIT.

The process of RIT begins with intravenous administration of the radiolabeled antibody in the patient's body. The antibody circulates through the plasma and is transported into the normal tissue surrounding the tumor across capillary walls. Once it is in the tissue, the antibody diffuses through and does not bind to the tissue in large amounts. It reaches the melanin antigen in the tumor and binds with the binding site to form an antibody-antigen complex. This complex emits the cytotoxic doses of radiation. Once the complex forms, it then dissociates into antibody and antigen, and some of the antibody in the tissue is cleared through lymphatic vessels.

This study aims to determine whether a 3D or 1D model is more accurate in assessing radial concentration levels of the various molecules present in the system. This study also aims to understand the antibody binding process and the effects of varying initial antigen concentrations on the RIT process.

Methods for the 3D Model

In order to generate the 3D model of the tumor within the tissue, two concentric spheres of radii 1.3 and 15 mm were constructed in COMSOL. The following mass transfer equations were used for the antigen, antibody, and antibody-antigen complex.

$$\frac{\partial c_i}{\partial t} + \nabla \cdot J_i = R_i \quad 1.1$$

$$J_i = -D_i \nabla c_i \quad 1.2$$

Since convection was not present in this model, this simplified to the following equation.

$$\nabla \cdot -D_i \nabla c_i = R_i \quad 1.3$$

The diffusion of the antibody in the tumor from the normal tissue was assumed to not affect the antibody concentration at the outer normal tissue surface because of the large tissue radius compared to the tumor radius. A zero-flux boundary condition was used at the outer surface of the normal tissue. The reaction terms for each of the three molecules were governed by equations.

For the antigen, the reaction term was

$$R_{Ag} = n(-k^+ C_{Ab} C_{Ag} + k^- C_{Ab-Ag}) \quad 2.1$$

where n is the valence of binding, 5, k^+ is the forward binding rate constant, $5.0E4 \text{ M}^{-1}\text{s}^{-1}$, k^- is the dissociation rate constant, $1.0E-5 \text{ s}^{-1}$. The diffusivity of antibody in the tumor is $4.16E-7 \text{ cm}^2\text{s}^{-1}$. The initial antigen concentration was 76000 nM within the tumor and 0 nM in the tissue.

For the antibody, the reaction term in the tumor was determined by the following equation.

$$R_{Ab,tumor} = k^+ C_{Ab} C_{Ag} + k^- C_{Ab-Ag} \quad 3.1$$

The reaction term in the tissue was

$$R_{Ab,tissue} = k^{bl} C_{Abp} - k^{ly} C_{Ab} \quad 4.1$$

where k^{bl} is the rate constant for uptake of antibodies into tissue from blood plasma, $4.6E-5 \text{ s}^{-1}$, and k^{ly} is the rate constant for removal of antibodies from the tissue by lymphatic clearance, $1.78E-6 \text{ s}^{-1}$. C_{Abp} is the concentration of antibodies in blood plasma, determined by the following equation.

$$C_{Abp} = C_{Ab0} e^{-\lambda t} \quad 4.2$$

where C_{Ab0} is the initial plasma concentration of 4.94 nM , and λ is $2.96E-5 \text{ s}^{-1}$. This equation was determined by exponentially curve fitting experimental data of C_{Ab0}/C_{Abp} over time, assuming first order clearance. The diffusivity of antibody in the tumor was $4.16E-7 \text{ cm}^2\text{s}^{-1}$, while the diffusivity in the tissue was $2.0E-7 \text{ cm}^2\text{s}^{-1}$. The initial antibody concentration was 0 nM in the tumor and the tissue.

Finally, for the antibody-antigen complex, the reaction term was the following.

$$R_{Ab-Ag} = k^+ C_{Ab} C_{Ag} - k^- C_{Ab-Ag} \quad 5.1$$

The initial complex concentration was 0 nM in the tumor and the tissue.

An extremely fine physics-controlled mesh was used, and the mesh density at the tumor-tissue interface is shown below in Figure 1. The model was solved from time zero to 72 hours with one-hour intervals. There were 1150382 total domain elements, and the computation time was 10 minutes and 10 seconds.

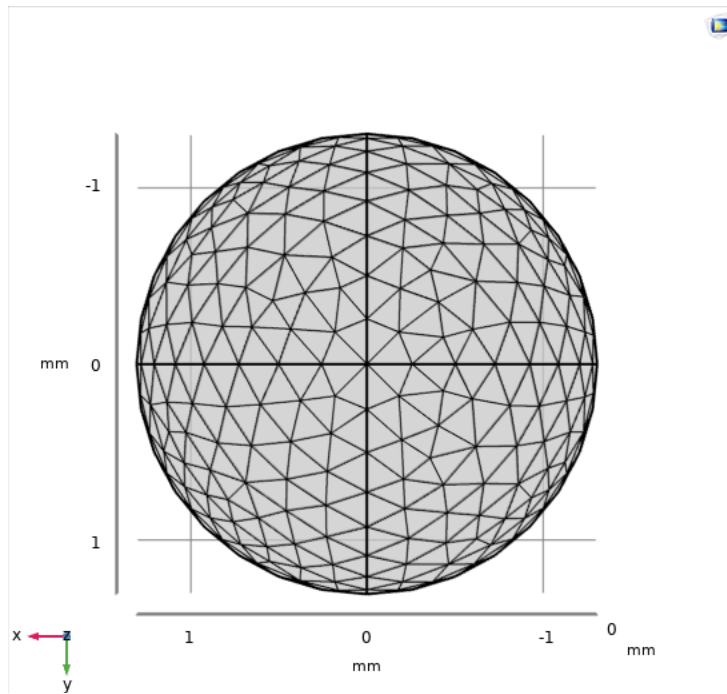


Figure 1: Mesh density at the tumor-tissue interface

Results of the 3D Model

The 3D model was developed to view radial concentrations of the three key molecules at 0, 24, 48, and 72 hours. Figures 2a, 2b, and 2c below illustrate the change in radial concentration of the antibody, antigen, and antibody-antigen-complex, respectively. Each of the molecule groups has been color-normalized across the 72 hours for ease of comparison. Additionally, negative concentration data was excluded from all of the plots for ease of comparison, but the very presence of negative concentration data indicates an inaccuracy within the model. This is due to an insufficient mesh density and will be discussed in further detail later.

Shown in Figure 2a, at 0 hours, the antibody concentration begins at 0 nM. Once it has diffused from the blood plasma to the tissue, at 24 hours, it is present in very high concentrations within the tissue, but as radial position approaches the tumor surface, antibody concentration gradually approaches 0 nM again. This is because the initial antigen concentration is so high, set at 76000 nM, that the antibody immediately binds to the antigen at the tumor-tissue interface and is therefore present in very low concentrations within the tumor itself. At 48 hours, less than half of the initial antibody concentration is present in the tissue, since a lot of the antibody has bound to the antigen within the tumor. Some of this concentration may also be due to the dissociation of the antibody from the complex, allowing the antibody to diffuse out of the tissue. Once again, antibody concentration within the tumor is 0 nM in this plot because all of the antibody has bound to the antigen at the tumor-tissue interface due to the high initial antigen concentration. Finally, at 72 hours, most of the antibody has diffused to the tumor-tissue interface and has bound to the antigen, so the antibody concentration across the entire tumor and tissue is now close to 0 nM. The small concentration of antibody within the tissue may be due to the forward binding reaction not being fully complete and may also be due to the dissociation of the antibody from the complex, allowing the antibody to be present in the tissue.

Shown in Figure 2b, radial antigen concentration is greatest within the tumor and approaches 0 nM outside of the tumor. Over the 72 hours, the antigen concentration within the tumor decreases slightly but remains otherwise unchanged. This is because the initial concentration of the antigen in the tumor is so high (76000 nM) that a majority of it remains even after all of the antibody has diffused to the tumor-tissue interface and bound to it.

Shown in Figure 2c, the antibody-antigen complex begins at a radial concentration of 0 nM at 0 hours because there is no antibody present yet to bind to the antigen. At 24 hours, there is a small antibody-antigen complex concentration at the tumor-tissue interface and slightly within the tumor boundary, since antibody has diffused to the interface and is now binding with the antigen. The antibody does not make it very far past the interface into the tumor because the initial antigen concentration is so high that the forward binding reaction occurs very quickly at the interface. The concentration of the complex at the interface increases at 48 hours as more antibodies diffuse to the interface, and there is only a slight increase from this concentration at 72 hours because most of the antibody has already been bound to the antigen, as seen in Figure 2a.

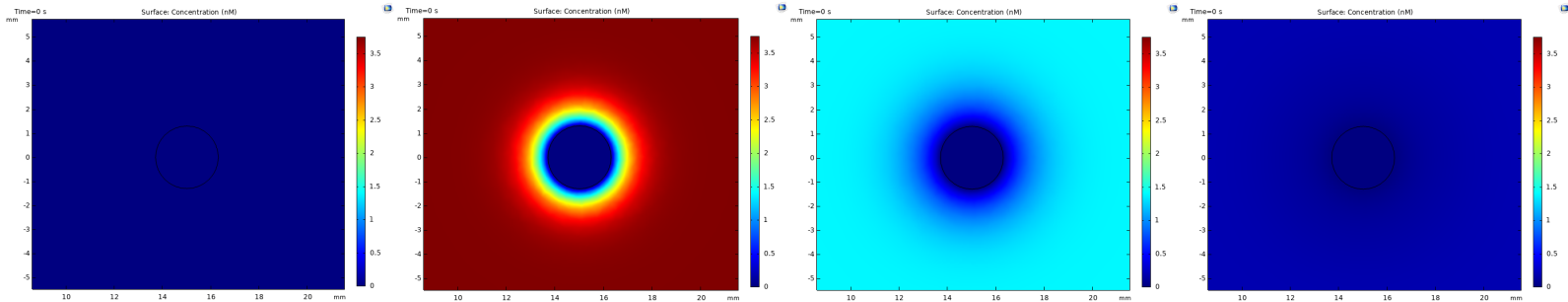


Figure 2a: Color-normalized [0, 3.75 nM] antibody radial concentration at 0, 24, 48, and 72 hours.

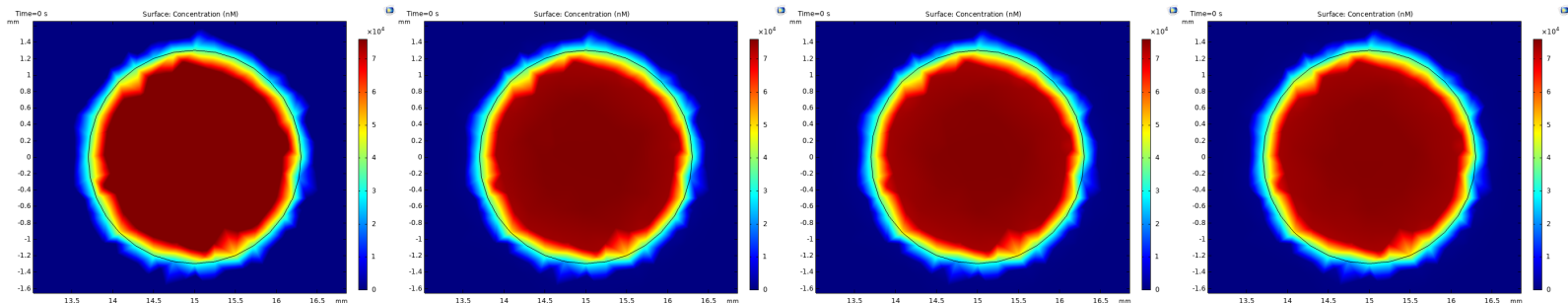


Figure 2b: Color-normalized [0, 76000 nM] antigen radial concentration at 0, 24, 48, and 72 hours.

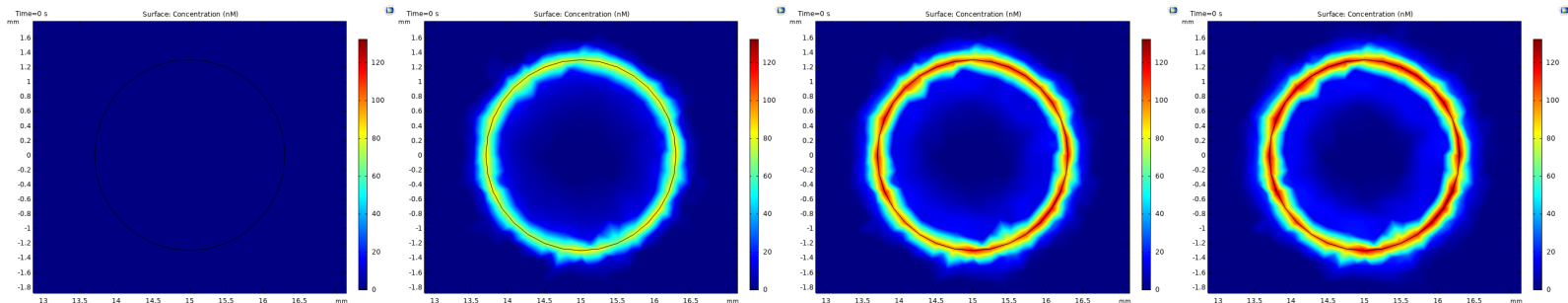


Figure 2c: Color-normalized [0, 132.47 nM] antibody-antigen complex radial concentration at 0, 24, 48, and 72 hours.

To graphically illustrate the change in radial concentration shown above, Figure 3 was created. It is clear from these graphs that as antibodies diffuse from the plasma through the tissue and reach the tumor-tissue interface over time where they begin binding to antigens, the antibody concentration within the tissue decreases, the antigen concentration within the tumor slightly decreases, and the antibody-antigen complex concentration at the interface increases. However, it is important to note that these graphs illustrate negative concentrations, most notably for the antibody-antigen complex. Negative concentrations are realistically impossible and indicate deficiencies within the 3D model. As previously mentioned, this is likely a result of a low mesh density that was not able to accurately resolve all of the equations to a high enough degree of accuracy.

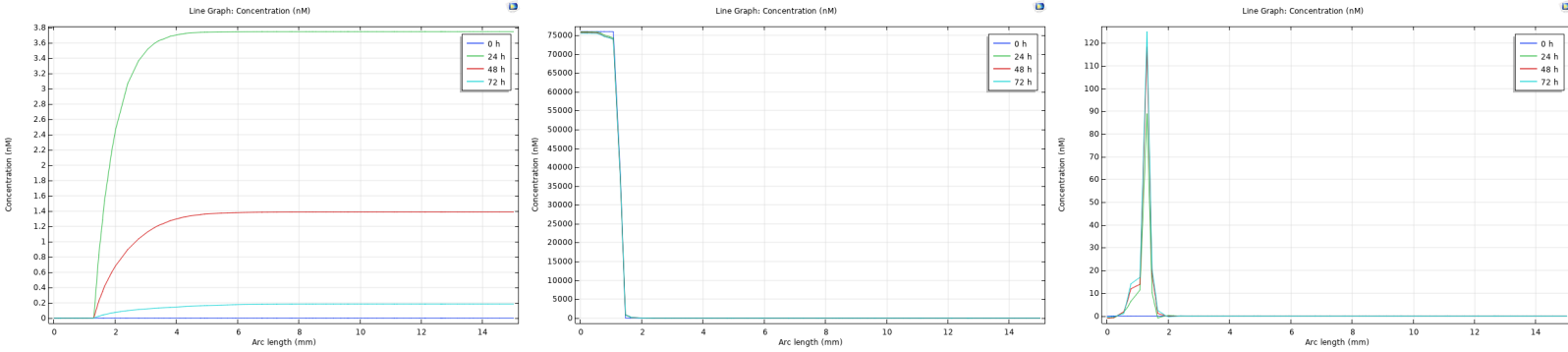


Figure 3: (left) Antibody, (middle) antigen, and (right) antibody-antigen complex radial concentration at 0, 24, 48, and 72 hours.

Corroborating the idea of a flawed model, Figure 4 below shows that the antibody-antigen complex concentration at the tumor-tissue interface is not uniform in the theta and phi directions. This is realistically inaccurate because there should be a uniform concentration across the tumor-tissue interface since it is a radially symmetrical sphere with consistent conditions across its surface. This further suggests that the mesh node density is not high enough to generate an accurate representation of radial concentration. A more accurate model would use a finer mesh that would have a much higher computational load and require significantly more time to generate. As a result, the 3D model is not ideal to analyze radial concentration, and the 1D model is likely sufficient to understand the problem.

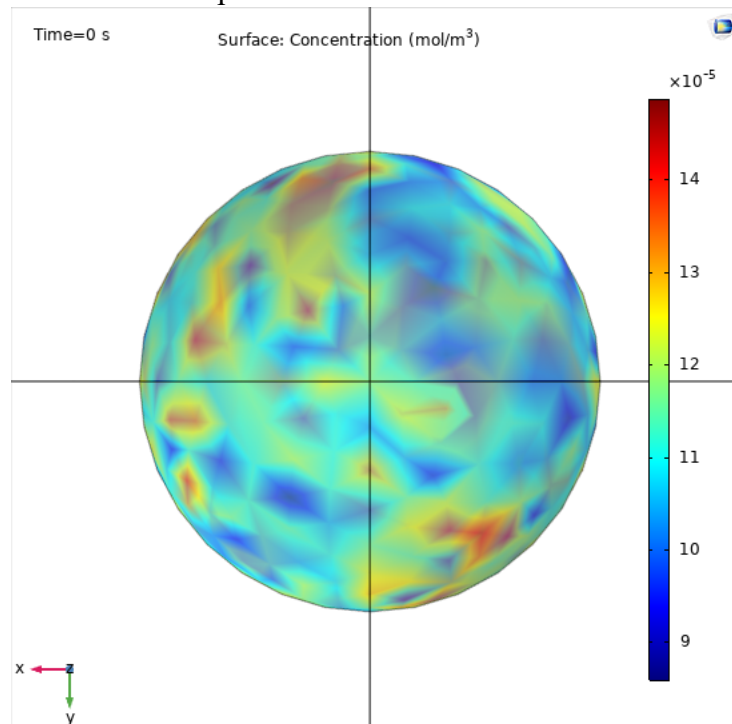


Figure 4: Antibody-antigen complex concentration at the tumor-tissue interface.

Methods for the 1D Model

Given the inaccuracies of the 3D model, the 1D model was created to reduce computational load and increase accuracy of results with a denser mesh. The system was modeled as a 1.3 mm line for the tumor and an adjacent 13.7 mm line for the tissue, creating a 15 mm radius for the tissue. A user-controlled mesh with a maximum element size of 0.0015 mm was used, and the 1D intervals in the computational domain are shown in Figure 5 below.

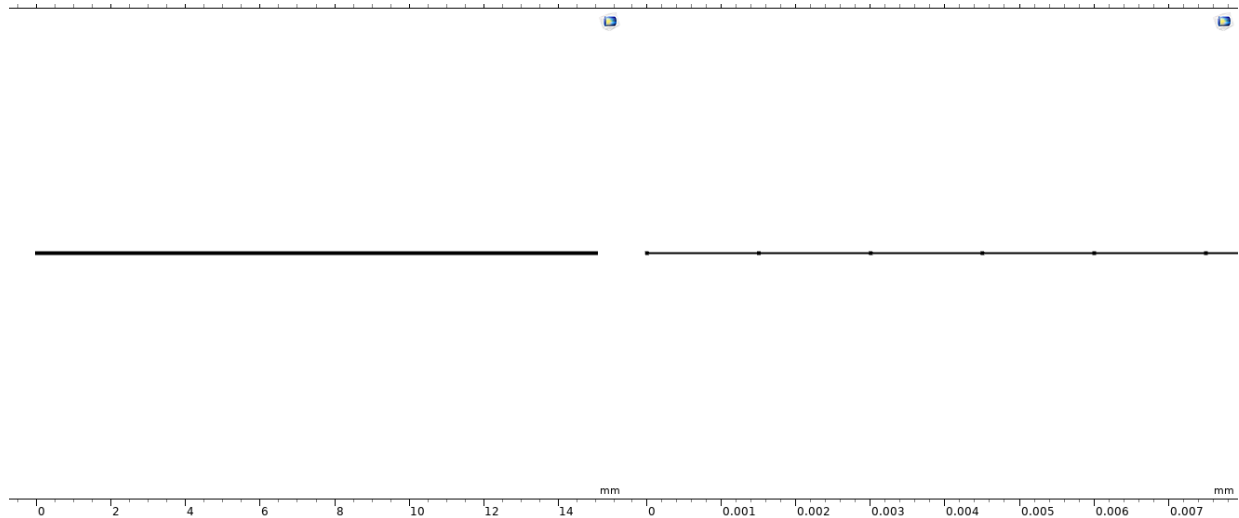


Figure 5: (left) Mesh for the 1D model. (right) Zoomed-in mesh displaying 1D intervals within the computation domain of the model.

The following partial differential equations were used for the antibody, antigen, and antibody-antigen complex.

$$e \frac{\partial^2 C}{\partial t^2} + d \frac{\partial C}{\partial t} + \nabla \cdot \Gamma = f \quad 6.1$$

$$\nabla = \frac{\partial}{\partial r} \quad 6.2$$

Γ is conservative flux, f is the source term, d is the damping coefficient, and e is the mass coefficient. Since there was no mass coefficient term for any of the molecules, the equation simplified to the following.

$$d \frac{\partial C}{\partial t} + \frac{\partial}{\partial r} \cdot \Gamma = f \quad 6.3$$

As with the 3D model, diffusion of the antibody in the tumor from the normal tissue was assumed to not affect the antibody concentration at the outer normal tissue surface because of the large tissue radius compared to the tumor radius. A zero-flux boundary condition was used at the outer surface of the normal tissue.

Using these governing equations, the conservative flux, source terms and damping coefficient were

$$\Gamma = 0 \quad 7.1$$

$$f = n(-k^+ C_{Ab} C_{Ag} + k^- C_{Ab-Ag}) \quad 7.2$$

$$d = 1 \quad 7.3$$

$$\frac{\partial C_{Ag}}{\partial t} = n(-k^+ C_{Ab} C_{Ag} + k^- C_{Ab-Ag}) \quad 7.4$$

where n is the valance of binding, 5, k^+ is the forward binding rate constant, $5.0E4 \text{ M}^{-1}\text{s}^{-1}$, k^- is the dissociation rate constant, $1.0E-5 \text{ s}^{-1}$. The diffusivity of antibody in the tumor is $4.16E-7 \text{ cm}^2\text{s}^{-1}$. The initial antigen concentration was 76000 nM within the tumor and 0 nM in the tissue.

The equations for the antibody in the tumor were

$$\Gamma = -D_{tumor} r^2 \frac{dC_{Ab}}{dr} \quad 8.1$$

$$f = r^2(-k^+ C_{Ab} C_{Ag} + k^- C_{Ab-Ag}) \quad 8.2$$

$$d = r^2 \quad 8.3$$

$$r^2 \frac{\partial C_{Ab}}{\partial t} + \frac{\partial}{\partial r} \left(-D_{tumor} r^2 \frac{dC_{Ab}}{dr} \right) = r^2(-k^+ C_{Ab} C_{Ag} + k^- C_{Ab-Ag}) \quad 8.4$$

where D_{tumor} is the diffusivity in the tumor, $4.16E-7 \text{ cm}^2\text{s}^{-1}$.

The equations for the antibody in the tissue were

$$\Gamma = -D_{tissue} r^2 \frac{dC_{Ab}}{dr} \quad 9.1$$

$$f = r^2(k^{bl} C_{Abp} - k^{ly} C_{Ab}) \quad 9.2$$

$$d = r^2 \quad 9.3$$

$$r^2 \frac{\partial C_{Ab}}{\partial t} + \frac{\partial}{\partial r} \left(-D_{tissue} r^2 \frac{dC_{Ab}}{dr} \right) = r^2(k^{bl} C_{Ab0} e^{-\lambda t} - k^{ly} C_{Ab}) \quad 9.4$$

where k^{bl} is the rate constant for uptake of antibodies into tissue from blood plasma, $4.6E-5 \text{ s}^{-1}$, k^{ly} is the rate constant for removal of antibodies from the tissue by lymphatic clearance, $1.78E-6 \text{ s}^{-1}$, and D_{tissue} is the diffusivity in tissue, $2.0E-7 \text{ cm}^2\text{s}^{-1}$. C_{Abp} is the concentration of antibodies in blood plasma, determined by the following equation.

$$C_{Abp} = C_{Ab0} e^{-\lambda t} \quad 9.5$$

where C_{Ab0} is the initial plasma concentration of 4.94 nM, and λ is $2.96E-5 \text{ s}^{-1}$. The initial antibody concentration was 0 nM in the tumor and the tissue.

Finally, for the antibody-antigen complex, the equations were the following.

$$\Gamma = 0 \quad 10.1$$

$$f = k^+ C_{Ab} C_{Ag} - k^- C_{Ab-Ag} \quad 10.2$$

$$d = 1 \quad 10.3$$

$$\frac{\partial C_{Ab-Ag}}{\partial t} = k^+ C_{Ab} C_{Ag} - k^- C_{Ab-Ag} \quad 10.4$$

The initial complex concentration was 0 nM in the tumor and the tissue.

The model was solved from time zero to 72 hours with one-hour intervals, and a parametric sweep was run for initial antigen concentrations of 76000, 7600, 760, 76, and 7.6 nM. There were 10001 total domain elements, and the computation time was 18 seconds, which was significantly lower than the computation time for the 3D model.

Results of the 1D Model

Primarily, in Figure 6, antibody concentration within the tumor and tissue was plotted as a function of radial distance for 2, 4, 8, 16, 24, 36, 48, 72 hours for five different initial antigen concentrations, 76000, 7600, 760, 76, and 7.6 nM. The graphs for 76000 and 7600 nM initial antigen concentrations are exactly the same, likely because the initial antigen concentrations are so high for both that the antigens in both setups are able to fully bind the antibodies once they reach the tumor-tissue interface, and there is excess antigen present. Moreover, the first three graphs with initial antigen concentrations of 76000, 7600, and 760 nM all follow the same trend in antibody concentration over time. In each, the antibody concentration is 0 nM within the tumor, and the concentration in the surrounding tissue is relatively uniform because complex formation takes place at the tumor-tissue interface due to the large binding rate constant. The concentration of the antigen in the tissue is low at 2 hours and slowly increases until it reaches its peak at 8 hours. Then, it falls back down at 16 hours and approaches 0 nM at 72 hours. This makes sense based on Equations 8.4 and 9.4 and lines up with the results found in the 3D model. Before 8 hours, the complex formation reaction at the tumor interface dominates because the forward binding rate constant is very large, $5.0E4 \text{ M}^{-1}\text{s}^{-1}$, while the diffusive flux is smaller and the lymphatic clearance has not yet gotten a chance to catch up with the rate of complex formation. However, between 8 and 16 hours, the diffusive flux through the tissue and dissociation reaction begins to dominate over the forward binding reaction, thus decreasing the overall antibody concentration in the tissue. Therefore, the diffusive flux, and thus the rate of removal and consumption, surpasses the complex formation rate, causing the antibody concentration in the tissue to decrease until it approaches 0 nM at 72 hours.

As initial antigen concentration decreases below 7600 nM, the maximum antibody concentration at several time points increases. This is because complex formation occurs more slowly since it is dependent on the concentration of the antigen, so when there are less antigens available to bind, the antibody is able to exist unbound for longer in the tissue. Moreover, for both the 76 and 7.6 nM initial antigen concentrations, the peak antibody concentration is reached at 16 hours rather than 8 hours because the antibody takes longer to bind since there are less available antigen binding sites. It is also important to note that as initial antigen concentration decreases, antibody concentrations at later times within the tumor itself increase above 0 nM and even above the antibody concentration within the surrounding tissue. This indicates that the antibody has reached the center of the tumor and the antigen binding sites are saturated because they cannot bind the antibodies as fast as the antibodies are diffusing through the tissue and tumor. In terms of Equation 8.4, this diffusion of the antibody into the tissue occurs because the diffusive flux term in the tumor finally becomes larger than the complex formation term when the antigen concentration is lower. For the 76 nM example, saturation begins at around 24 hours, and for the 7.6 nM example, saturation begins as early as 4 hours. It begins earlier in the 7.6 nM example because the antigens become very quickly saturated with such a low initial antigen concentration.

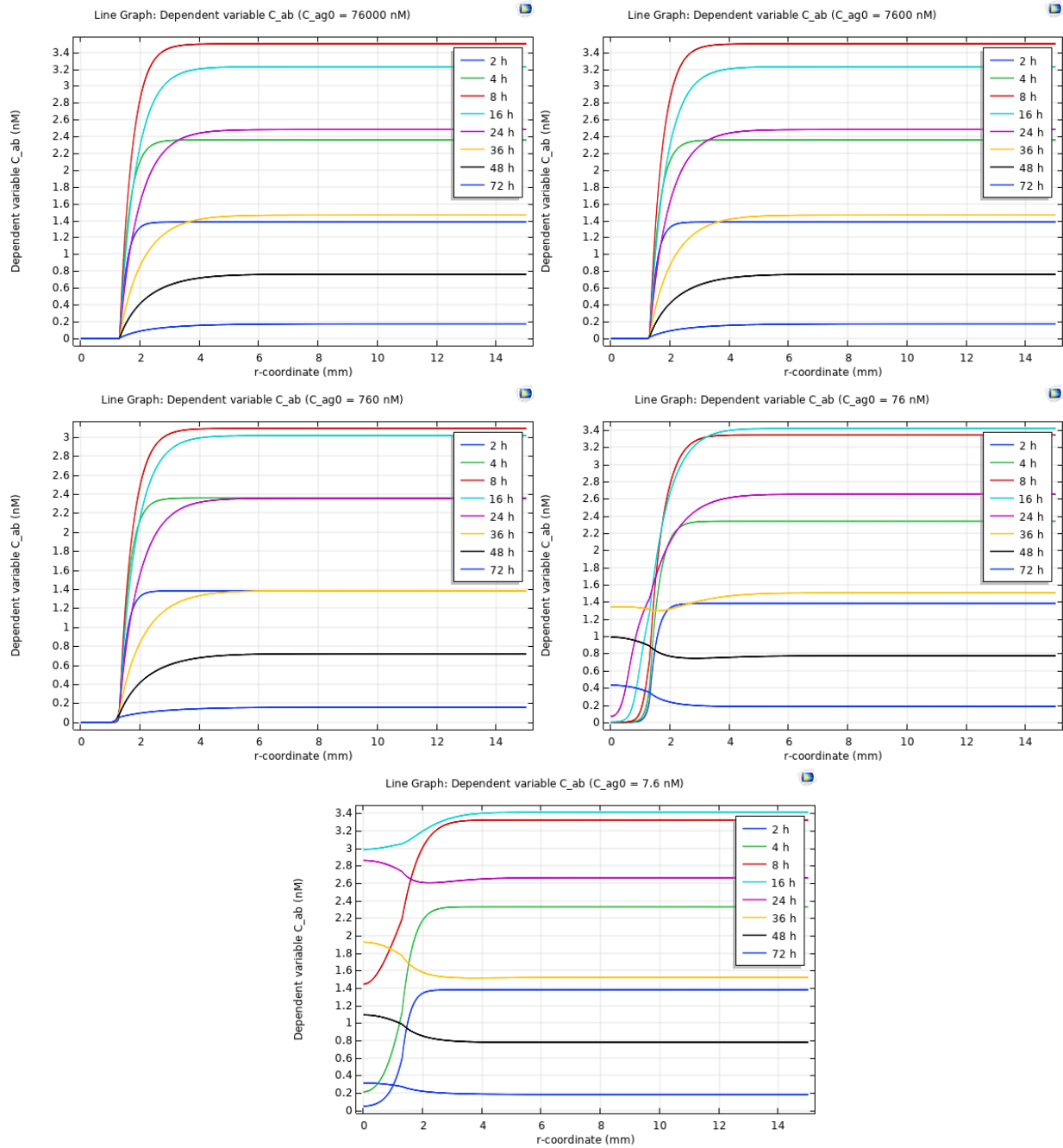


Figure 6: Antibody concentration within the tumor and tissue as a function of distance for 2, 4, 8, 16, 24, 36, 48, 72 hours for 76000, 7600, 760, 76, and 7.6 nM initial antigen concentrations.

Furthermore, Figure 7 illustrates the antibody-antigen complex concentration as a function of distance at 72 hours. For low initial antigen concentrations of 7.6 and 76 nM, the radial concentration of the complex remains close to zero and relatively constant throughout the tumor. This is because at 72 hours, the antibody has already fully penetrated the tumor and bound to the antigens present. There is no more antibody entering the tissue or diffusing to the tumor, and most of the antibody has already been used to create the complex. Therefore, the only reaction that is occurring is the dissociation of the complex, via Equation 10.4. As a result, the

complex concentration is uniform throughout the tumor. It is very close to 0 nM for the 7.6 nM initial antigen concentration because most of the complex has dissociated.

For an initial antigen concentration of 760 nM, the complex concentration towards the center of the tumor is close to 0 nM and increases radially as it approaches the tumor-tissue interface because this is where most of the complex formation occurs since the antigen concentration is high enough and there are antigens present to bind. However, this concentration reaches a plateau at the interface because there is not enough antigen present to bind all of the antibodies, so the antigen becomes almost fully saturated, and the complex concentration can only reach a value of around 95 nM. For an initial antigen concentration of 7600 nM, the complex concentration towards the center of the tumor is similarly close to 0 nM and increases radially as it approaches the interface. However, the concentration does not plateau; it instead increases to around 500 nM. This same behavior applies for the initial concentration of 76000 nM, except the complex concentration exponentially increases even more at the tumor-tissue interface to about 1800 nM because the antigens can bind all of the antibodies immediately at the surface. In cases of high antigen concentration, the antigen binding sites do not become saturated within 72 hours.

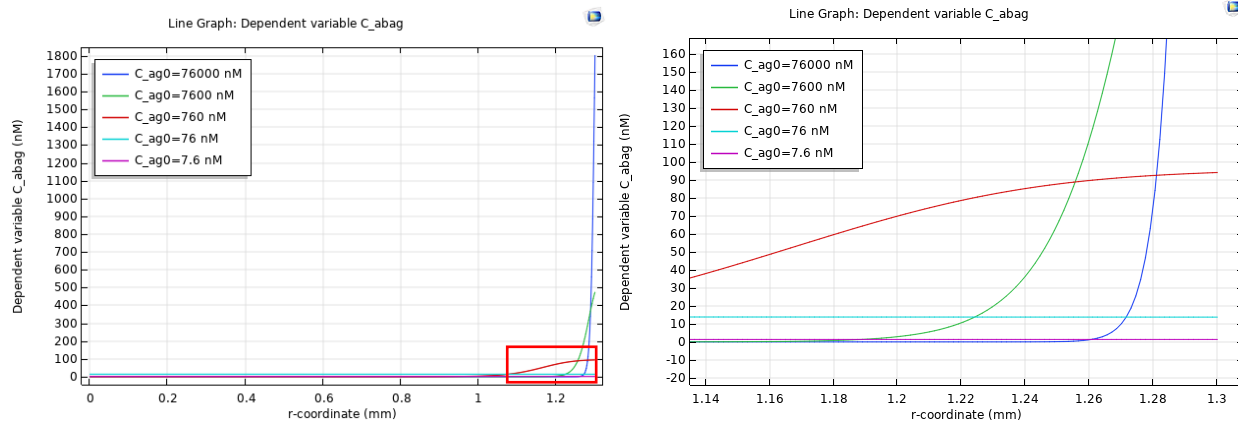


Figure 7: (left) Antibody-antigen complex concentration as a function of distance at 72 hours. (right) Zoomed-in view of graph from 1.14 to 1.3 mm radial distance.

For each of the initial antigen concentrations tested, the radial distance and volume of the tumor penetrated at 72 hours were calculated and reported in Table 1 below. The radial distance penetrated is said to occur when the complex concentration reaches 1 nM, indicating that the antibody has sufficiently penetrated the tumor. The table shows that the radial distance penetrated and thus the volume of the tumor penetrated increases as the initial antigen concentration decreases. At very low antigen concentrations of 76 and 7.6 nM, the antibody is able to penetrate nearly 100% of the tumor. This makes sense based on Equation 8.4 because diffusive flux through the tumor dominates over complex formation as antibody concentration decreases. Antibodies are able to diffuse deeper into the tumor since there are less antigen binding sites available to bind them and form complexes. For high initial antigen concentrations, however, complex formation dominates over diffusive flux, so much of the antibody binding occurs at the surface of the tumor, and the antibody thus does not penetrate as deeply into the tumor.

Table 1: Radial Distance and Volume of Tumor Penetrated at 72 hours for Different Initial Antigen Concentration

Initial Antigen Concentration (nM)	Radial Distance Penetrated (mm)	Volume of Tumor Penetrated (%)
76000	0.0405	9.05
7600	0.1155	24.35
760	0.3554	61.63
76	1.3	100
7.6	1.3	100

In order to determine the time at which the peak complex concentration in the radial position begins to decrease, Figure 8 was created to show peak complex concentration over time. The time at which peak complex concentration begins to decrease was estimated to be about 40 hours by zooming into the graph. At this time, the plasma antibody concentration is close to 0 nM and the rate of complex dissociation and lymphatic clearance is surpassing the rate of transport from the plasma, as seen in Equation 9.4. This will be described in more detail in the Discussion.

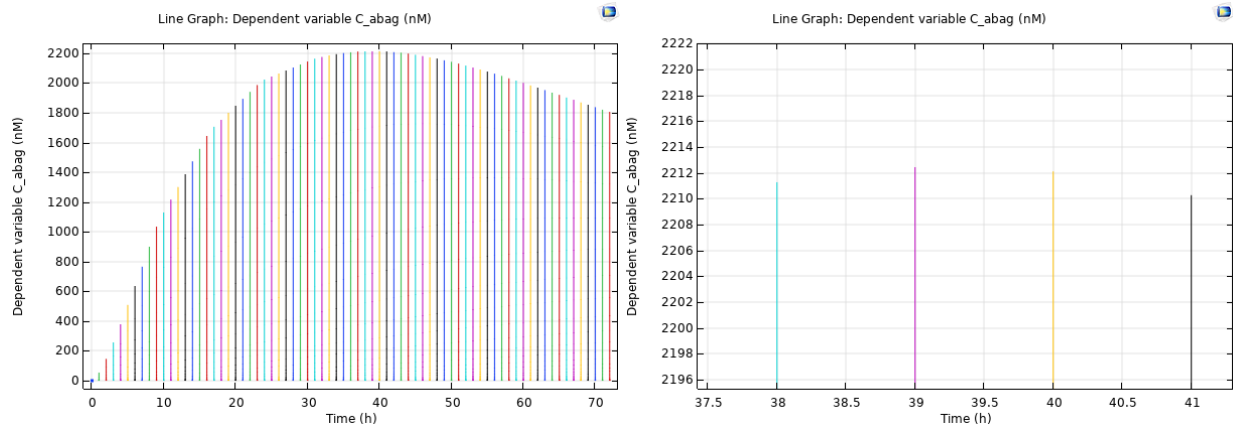


Figure 8: (left) Peak concentration of antibody-antigen complex over 72 hours. (right) Zoomed-in view of graph where peak concentration decreases at 40 hours.

Figure 9 shows a graph of the average complex concentration within the tumor at 2, 4, 8, 16, 24, 36, 48, 72 hours for each of the antigen concentrations tested. This was found using the line average function in COMSOL. For initial antigen concentrations of 76000, 7600, and 760 nM, the complex concentration begins at 0 nM at 0 hours, very quickly increases until about 20 hours, and then increases more slowly until 72 hours. This makes sense because the antibody is present in high concentrations at the beginning, so complex formation occurs rapidly, and the concentration of the complex therefore increases rapidly. Once the antibody concentration in the tissue has decreased because a large amount has already bound to antigens, the rate of complex formation decreases, so the concentration of the complex therefore increases less quickly. The complex concentration increases throughout the entire time period because the forward binding reaction dominates over the backward one, as seen in Equation 10.4. The 760 nM condition yields a slightly larger average complex concentration than the two larger initial antigen concentrations because the antibody is able to penetrate slightly more of the tumor's volume in the 760 nM case, so complex formation occurs not only on the tumor surface but also slightly

deeper inside the tumor. Therefore, the average complex concentration across the entire volume of the tumor is slightly higher.

For the lower initial antigen concentration of 76 nM, the complex concentration increases much more rapidly than for the higher initial concentrations and then reaches a plateau and begins to decrease slightly. The initial increase is greater than that of the three higher initial antigen concentrations for the same reason previously mentioned– the antibody is able to penetrate the tumor more, so complex formation can occur deeper inside the tumor, and the average complex concentration across the tumor volume is therefore larger. The plateau occurs either because all of the antibody has been used up and bound to the antigens or because all of the antigens are saturated. However, it is more likely the case that the antigens are fully saturated since this would occur sooner than the antibodies would be used up because of the very low initial antigen concentration. The slight decrease at the end of this curve towards 70 hours is likely because there is no more antibody left in the tissue to bind with the antigen once the antigen has dissociated from the complex because a lot of the antibody has been removed through lymphatic clearance.

Finally, for the lowest initial antigen concentration of 7.6 nM, the complex concentration slightly increases and then quickly plateaus at a low value of less than 2 nM. This is because the initial antigen concentration is so low that any time an antigen dissociates from a complex, it immediately binds to an antibody, so the concentration of the complex is kept at a relatively constant value since the antigen remains saturated throughout the 72 hour period.

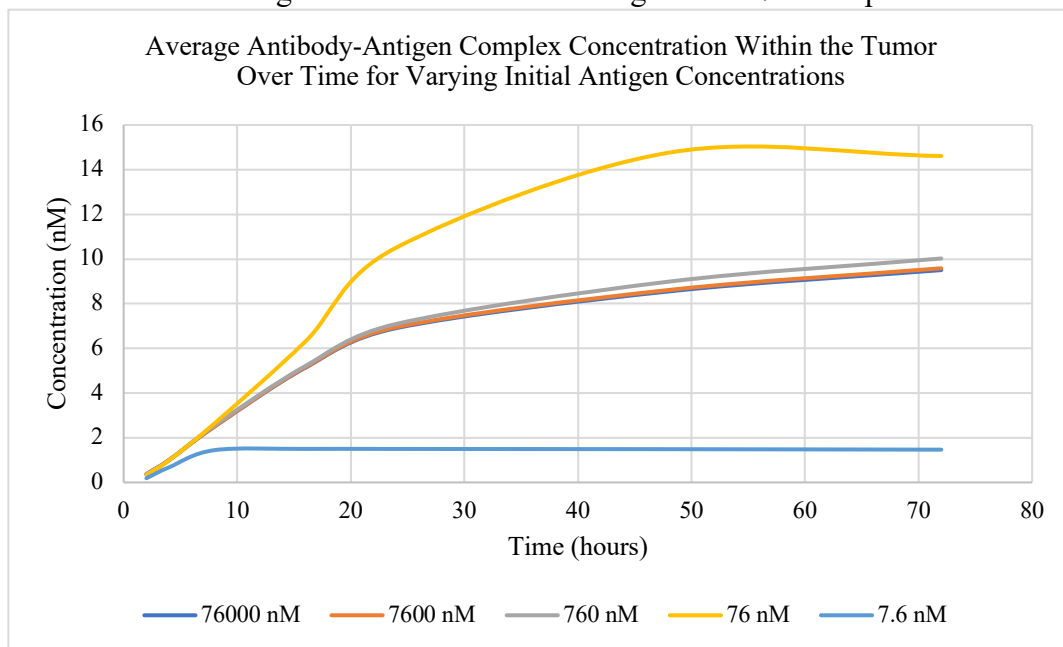


Figure 9: Average antibody-antigen complex concentration within the tumor at 2, 4, 8, 16, 24, 36, 48, 72 hours for varying initial antigen concentrations of 76000, 7600, 760, 76, and 7.6 nM.

Discussion

Saturation of the antigen binding sites at the tumor's periphery can be defined as any time when the antigen concentration at the tumor's surface (1.33 mm) reaches 0 nM. Figure 10 below show the radial antigen concentration within the tumor for initial antigen concentrations of 760, 76, and 7.6 nM. From these graphs, it is clear that only the 760 and 76 nM initial conditions allow the antigen to reach 0 nM at the surface, so antigen saturation at the tumor's periphery only occurs for these two initial concentrations.

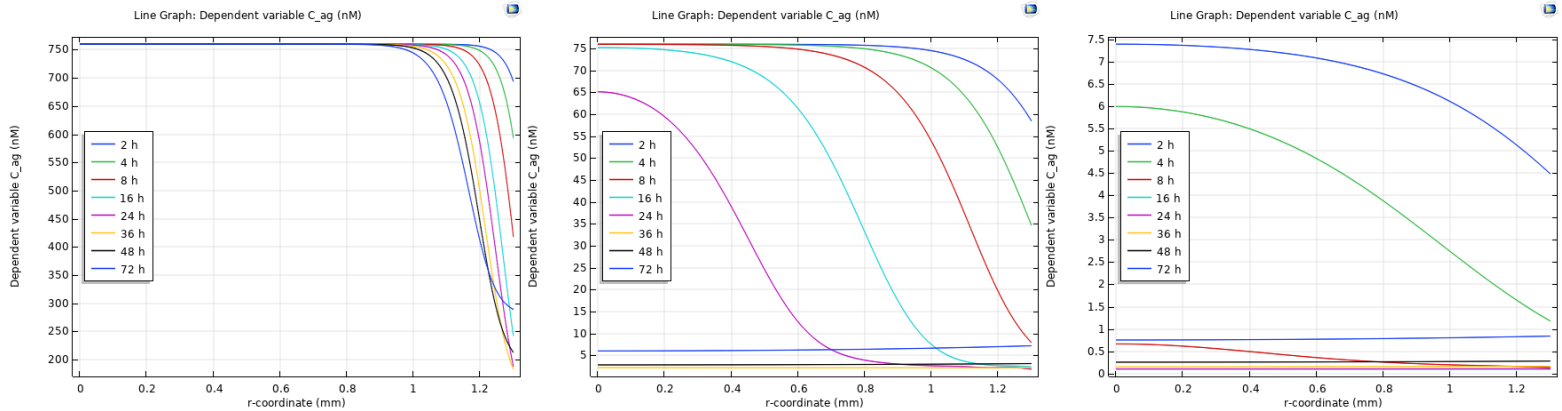


Figure 10: Radial antigen concentrations within the tumor at 2, 4, 8, 16, 24, 36, 48, 72 hours for initial antigen concentrations of (left) 760, (middle) 76, and (right) 7.6 nM.

Saturation of the antigen binding sites throughout the entire tumor can be defined as any time when the antigen concentration at the center of the tumor is equal to 0 nM, indicating the antibody has fully penetrated the tumor since the antigens cannot bind the antibodies fast enough because the initial antigen concentration is not high enough. Full antibody penetration of the tumor occurs for initial antigen concentration of 76 and 7.6 nM, as seen in Table 1 so these are the two initial concentrations that yield saturation throughout the entire tumor. There is an excess of melanin when the initial concentration of melanin is 76000 and 7600 nM. This can be seen in Figure 6 because the graphs for antibody concentration for these two initial antigen concentrations are exactly the same, indicating that adding more antigen to the 7600 nM does not increase complex formation or decrease antibody concentration, so there is already an excess of antigen with an initial concentration of 7600 nM.

For a melanin concentration of 76000 nM, the peak antibody-antigen complex concentration begins to decrease at about 40 hours, as seen in Figure 8. This occurs because the plasma antibody concentration is close to zero and the rate of complex dissociation and lymphatic clearance is surpassing the rate of transport from the plasma, as seen in Equation 9.4. In actuality, the plasma antibody concentration falls to around zero after about 24 hours, based on the exponential decay in Equation 9.5. When the equation is rearranged to solve for time, it becomes $t = -\frac{1}{\lambda} \ln \frac{C_{Abp}}{C_{Ab0}} = -\frac{1}{2.96E-5 s^{-1}} \ln \frac{C_{Abp}}{4.94 nM}$. When C_{Abp} approaches 0 nM, t approaches 24 hours. However, the complex concentration still continues to increase past that point until 40 hours because the rate of complex formation, $k^+ C_{Ab} C_{Ag}$, is a second-order reaction, and the forward binding constant is so large that it dominates over the complex dissociation reaction. However, once the complex dissociation and lymphatic clearance begins dominating at 40 hours, the peak complex concentration begins to decrease.

Antineoplastic therapy with cytotoxic agents is used to treat cancer and works by binding to surface proteins of cancerous cells and promoting inappropriately stable, non-functional cellular structure development. Cytotoxic agents can result in depolymerization, dissolution of key cellular components, suppression of normal cell dynamics, and more (Ismael et al., 2008). This means that in the context of a cancerous tumor, a cytotoxic agent could likely destroy antigen binding sites on the cancerous cells. This would consequently decrease the concentration of functional melanin binding sites. If radiolabeled antibodies were then administered into the patient's blood, they would cross into the tissue and more quickly saturate the melanin binding sites. Therefore, there would be saturation of the melanin binding sites throughout a larger percentage of the tumor, as shown in Table 1, which would allow the complex to form deeper in the tumor and deliver the radioimmunotherapy throughout the entire mass. Once the antibodies have attached to the antigen binding sites deep in the tumor and administered the radioimmunotherapy, eventually dissociating from the complex, it would be wise to destroy more of the antigen binding sites with cytotoxic agents so another treatment of radiolabeled antibodies can penetrate the entire tumor again and destroy the remaining antigens. Therefore, it would be best to administer antineoplastic therapy with cytotoxic agents first, followed by RIT, and then to repeat the process until the tumor has been destroyed.

Summary of Peer-Reviewed Journal Article

Background

Many diseases are caused by the deterioration of brain function, including neurological disorders, encephalitis, multiple sclerosis, tumors, and strokes (Hassanzadeganroudsari et al., 2020). Despite the burgeoning development of novel therapeutic systems for brain diseases, many of these treatments have low efficacy due to difficulty crossing the blood brain barrier (BBB), a layer of endothelial cells that seal off the vascular lumen from the abluminal side where the brain resides. The BBB has a unique chemical, immunologic, and functional environment because it prevents leukocytes, neuro-toxic macromolecules, and bacteria in the blood from accessing the brain interstitial fluid. The BBB does not have trans- or para-cellular channels, so molecules in the blood must cross through receptor-mediated transport or lipid-mediated free diffusion. Currently, transport efficiency is evaluated with unreliable in vivo and computational models that have hindered the development of efficient central nervous system (CNS) drugs.

Understanding the physiological and biological systems of the BBB can improve this. One technique that would greatly benefit from this deeper understanding is nano-drug delivery since nanoparticles can effectively penetrate the BBB and CNS. In order to determine a drug's impact on the target site, drug distribution at the target must be understood so that a sufficient concentration of the drug can be delivered for effective treatment. Since the human brain is inaccessible for sampling, mathematical models are useful in understanding drug distribution in the brain and can have significant clinical implications. A model to describe the interaction between a drug and nano-carrier and the BBB is particularly useful in developing effective drug delivery treatments.

Goal

The goal of this study is to analyze mass transfer of nanoparticles across the blood brain barrier through the basement membrane, endothelial cells, and astrocytes foot process. To do this, the engineers develop two-dimensional (2D) and three-dimensional (3D) models that evaluate the mass transfer rate in blood brain capillaries. The data obtained from the models can then be used to determine the concentration of drug necessary to reach a target distance across the BBB. The study then validates the simulation results by comparing them to experimental data for nanoparticle mass transfer resistance in the capillary across a wide range of red blood cell distances. Another goal of the model is to create an accurate mesh that reduces computational error. Ultimately, the study aims to determine the systemic drug concentration needed to reach a set target distance across the BBB.

Numerical Analysis

This study used COMSOL Multiphysics software for the 2D and 3D models, and computational time for solving the principal equations was approximately 7 minutes. Three membranes of the BBB were modeled as resistors in series. The basement membrane is the first point of contact with the circulatory system and has the largest amount of mass transfer from the capillaries. The endothelial cell layer is composed of endothelial cells with tight junctions between them which allow for the distribution of substances. The selective movement of particles between these cells is assumed to be a constant variable. The final layer is the astrocytes foot process, which is above the neural cells and acts as a tight interconnected network.

Several assumptions were made about the fluid dynamics of this problem. The blood was assumed to behave as a Casein fluid and the flow in the capillary was assumed to be laminar,

based on a Reynolds number of 0.008 within the capillary. The nanoparticles are immersed in the plasma and enter the basement membrane via diffusion through the capillary walls. The capillary diameter ranged from 8 to 16 μm , the geometry of the model was assumed to be axisymmetrical, and the capillary environment was assumed to be about 80% of the total geometry while the capillary space accounted for 20% of the total geometry. Moreover, the study assumes that the blood stream flows continuously through the capillaries and is not disrupted by capillary intake.

The basic governing equations for flow within the capillary are the following.

$$\begin{aligned}\nabla u &= 0 \\ \frac{\partial u}{\partial t} + u\nabla(u) &= -\frac{1}{\rho}\nabla(p) + \vartheta\nabla^2 u \\ \frac{\partial c}{\partial t} + u\nabla C &= \nabla(D\nabla C)\end{aligned}$$

In these equations, u is velocity, ϑ is viscosity, C is concentration, and D is diffusion coefficient. Moreover, the governing equations for mass transfer around the capillary porous media are the following.

$$\begin{aligned}\nabla u &= 0 \\ \frac{\partial u}{\partial t} + u\nabla\left(\frac{\mu}{\varepsilon}\right) &= -\frac{1}{\rho}\nabla(\varepsilon p) + \vartheta\nabla^2 u + F \\ \varepsilon\frac{\partial c}{\partial t} + u\nabla C &= \nabla(D_m\nabla C), D_m = \varepsilon D\end{aligned}$$

In these equations, ε is the porosity coefficient and F is the external force due to the porous medium, calculated through the following equation.

$$\begin{aligned}F &= -\frac{\varepsilon v}{k_{darcy}} - \frac{\varepsilon F_\varepsilon}{\sqrt{k_{darcy}}} |u|u \\ F_\varepsilon &= \frac{1.75}{\sqrt{150\varepsilon^3}} \\ k_{darcy} &= \frac{\varepsilon^3 d_p^2}{150(1-\varepsilon)^2}\end{aligned}$$

Here, d_p is the diameter of the solid particles in the porous medium. All of these parameters in the equations were acquired from past experimental work and computational modeling. Some of these parameters included the radii of capillaries, endothelial cells, the basement membrane, the astrocyte foot process cells, neurons, red blood cells (RBCs), and nanoparticles. In addition, they used blood velocity, viscosity, and density, all commonly accepted values in literature, and nanoparticle viscosity and density.

The boundary condition used on the capillary wall defines absorption of the nanoparticles from the wall. This boundary condition is set as the following.

$$-D\frac{\partial c}{\partial y} + u_w c_w = k c_w$$

In this equation, k is the permeability of the capillary wall and D is the diffusion coefficient. This equation makes sense when it is considered as a mass balance. The mass of nanoparticles inside of the capillary wall, defined as velocity multiplied by concentration, minus the diffusive flux through the capillary wall and the out term, defined as permeability multiplied by the concentration in the capillary wall is equal to zero because there is no accumulation at the wall. This makes sense given the system that is being modeled. Moreover, a zero-flux boundary condition was set at the middle of the capillary, which makes sense because of symmetry, and

the edge of the region of neurons, which makes sense because nanoparticles do not flow past this point in the model. A constant velocity in the radial direction of the capillary was also assumed, which is a reasonable assumption to model with one-dimensional fluid flow.

Major Results

Primarily, the engineers validated their model by comparing simulated data with experimental data and found only 6% average deviation, suggesting an accurate model. The capillary section of the 2D and 3D models revealed that the passage of nanoparticles in the presence of red blood cells leads to a significant reduction in the drug concentration in the capillary from 0.5 to 0.1 mol/m³. In other words, the number of red blood cells has a significant impact on drug concentration close to the wall, so the greater the red blood cells, the lower the concentration of the drug inside the capillary. A concentration plot of nanoparticle flow in the capillary is shown for the 3D model in Figure 11 below. Moreover, the concentration of nanoparticles was remarkably reduced from 0.4 to 0.1 mol/m³ after passing through the endothelial cell layer, suggesting that this layer has significant resistance because of the tight junctions between endothelial cells.

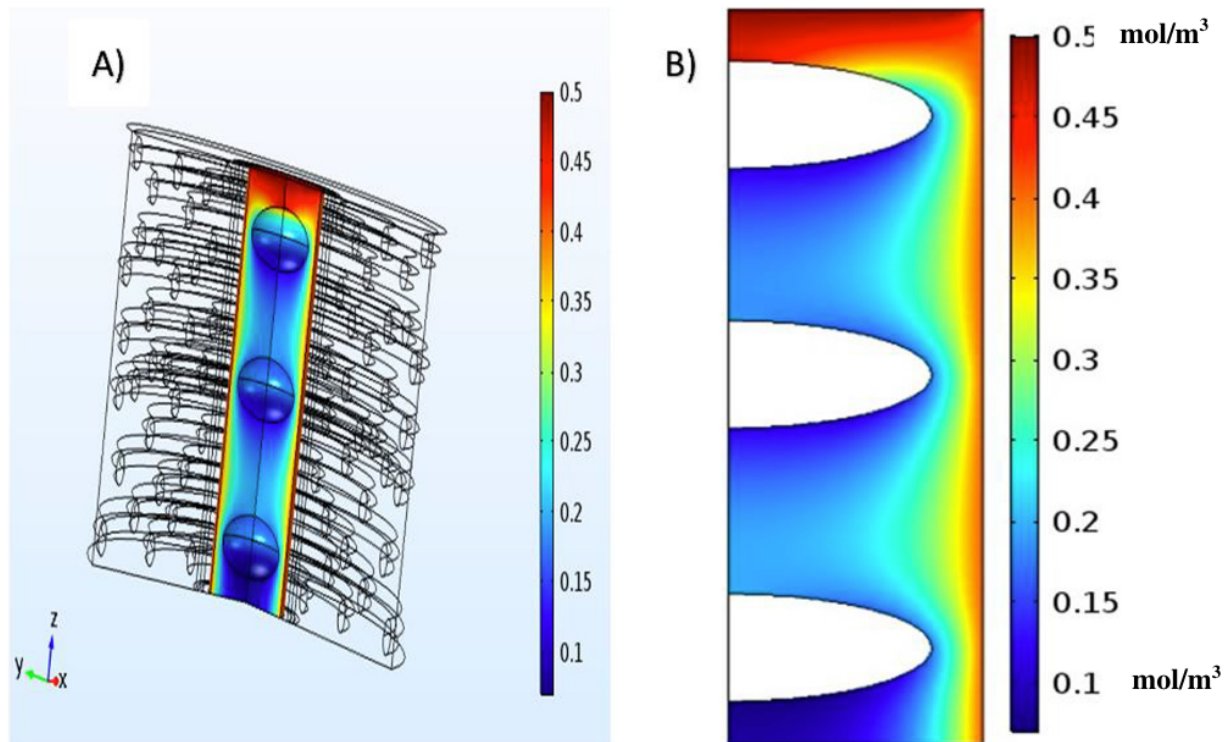


Figure 11: Nanoparticle concentration plot within the capillary. White spaces in Figure B indicate red blood cells. Figure adapted from Hassanzadeganroudsari et al., 2020.

After passing through the basement membrane of the BBB, the concentration of the nanoparticles decreased by 0.02 mol/m³, suggesting a lower mass transfer resistance as compared to the endothelial cell section. The astrocyte layer of the BBB further reduced the concentration of nanoparticles by 0.02 mol/m³ because mass diffusion through this layer is similar to that of the basement membrane. The transfer of the nanoparticles through the neurons resulted in a 0.01 mol/m³ decrease, bringing the concentration down to 0.04 mol/m³ at this point in the model. This region also revealed that a greater number of neurons leads to a greater reduction in nanoparticle

concentration. Nanoparticle concentration through the four post-capillary layers discussed is shown in Figure 12 below.

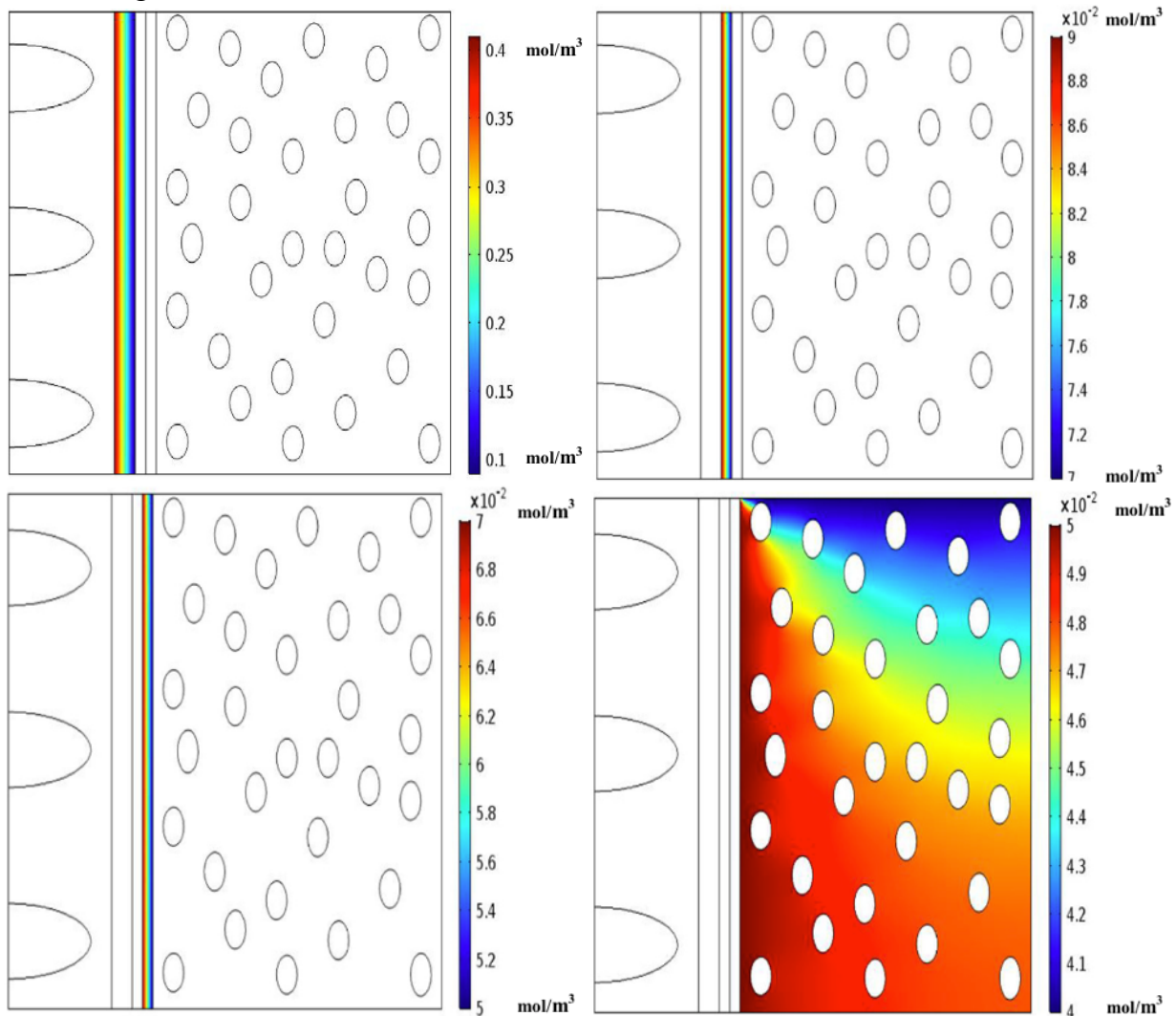


Figure 12: Nanoparticle concentration in the (top left) endothelial cell layer, (top right) basement layer, (bottom left) astrocyte layer, and (bottom right) neurons. Figure adapted from Hassanzadeganroudsari et al., 2020.

The engineers also analyzed the effect of capillary diameter on the concentration and diffusive flux of nanoparticles, finding that an increase in capillary diameter from 0.5 to 3.5 μm decreased the concentration of nanoparticles in the capillary from 0.42 to 0.20 mol/m³. This is due to a greater dispersion of nanoparticles in a larger capillary, thus decreasing the concentration. The study also found that the diffusion coefficient of the nanoparticles was inversely proportional to the capillary diameter, so an increase in capillary diameter reduced the diffusion flux and thus the amount of mass transfer in the capillary, in accordance with Fick's Law. In addition, the study found that increasing the distance between the neurons and the capillary wall dramatically reduces the concentration of nanoparticles within the neurons since there is more tissue for the particles to diffuse through before reaching the neurons. Finally, the study found that increasing the blood flow velocity from 0.1 to 5 mm/s results in a significant

concentration reduction at the neurons because the nanoparticles in the blood cannot diffuse as much through the capillary wall.

Limitations/Future Work

There were several limitations to this study's analysis. Primarily, many broad assumptions were made that may have skewed the results. For example, the nanoparticles and RBCs were assumed to be spherical, which is not entirely true in reality. The study also did not compare results from the 2D and 3D model and simply conglomerated all of the data into one analysis. It would be valuable to understand the differences in the setups and results of these models. The geometry was also ill-defined and mass transport through the various layers themselves was poorly characterized, since the governing equations mostly applied to transport across the capillary wall. In addition, laminar flow in the capillary was assumed, but this is not necessarily true if the capillary has branches or if the model views the beginning or end of the capillary. Another assumption that may not be true is the lack of interaction between the nanoparticles and the tissue surrounding the neurons. Some of the nanoparticles may be stopped by interactions with extracellular components, which will reduce concentration in the neurons. Additionally, a no-slip condition between the blood and the capillary wall would have made the modeling of blood flow and thus nanoparticle movement within the capillary more accurate. Moreover, despite the governing equations of concentration with respect to time, the results section made no mention of concentration changes over time. The only results mentioned were regarding concentration with respect to position. Analyzing concentration changes over time would be incredibly valuable for understanding how long it requires for the drug to diffuse across blood brain barrier and reach the patient's brain. It would also have been valuable to alter the nanoparticle concentration within the blood and determine the effect on mass transfer to the neurons.

References

- Hassanzadeganroudsari, M., Soltani, M., Heydarinasab, A., Nakhjiri, A. T., Hossain, M. K., & Khiyavi, A. A. (2020). Mathematical modeling and simulation of molecular mass transfer across blood brain barrier in brain capillary. *Journal of Molecular Liquids*, 310, 113254. doi:10.1016/j.molliq.2020.113254
- Ismael, G. F., Rosa, D. D., Mano, M. S., & Awada, A. (2008). Novel cytotoxic drugs: Old challenges, new solutions. *Cancer Treatment Reviews*, 34(1), 81-91. doi:10.1016/j.ctrv.2007.08.001